J Eng Math (2017) 107:19–35
DOI 10.1007/s10665-017-9933-7

Micro-slot injection into a boundary layer driven by a favourable pressure gradient

A. J. Williams · **R. E. Hewitt**

Received: 28 February 2017 / Accepted: 8 August 2017 / Published online: 16 September 2017

Abstract We investigate the effects of injection through a streamwise-aligned 'micro-slot' into a laminar boundary layer driven by a favourable pressure gradient of power-law type. The injection slot exists at all downstream locations, and is 'micro' in the sense that it has a finite spanwise width that is a fixed ratio of the local boundary-layer thickness. This approach is motivated by recent studies of micro-jets (of small spanwise and streamwise extents), which have indicated that for short spanwise scales, injection does not necessarily lead directly to separation. Injection in the absence of a free-stream pressure gradient has recently been analysed by Hewitt et al. (J Fluid Mech 822:617–639, 2017), and here we show that boundary layers in a favourable pressure gradient behave qualitatively differently. We present three-dimensional boundary-layer solutions affected by slot injection and contrast these with the corresponding zero pressure-gradient states. In the absence of a pressure gradient, injection results in low-speed streamwise-aligned streaks, where the amplitude and spanwise width of the injection determine the geometry of the streaks as one of the three possible types. The introduction of a favourable pressure gradient greatly reduces the spanwise extent of injection-driven streaks and removes the delineation between the three distinct flow regimes found in the zero pressure-gradient case. We present an asymptotic description in the limit of a large injection-slot width, thereby approaching the macro-slot limit from the micro-slot formulation. This description shows that not all injection rates and pressure gradients recover the expected Falkner–Skan solution at the centreline of the injection slot in the macro-slot limit. We explain this disagreement in terms of local spatial (cross flow) eigenmodes that are associated with a cross-flow collisional process at the centre of the injection slot.

Keywords Boundary-layer · Injection · Pressure gradient · Short spanwise scale

Mathematics Subject Classification 76D10

1 Introduction

There has, recently, been increased interest in the use of micro-jets as an active mechanism to control flow separation; see, for example, the experiments of Kumar and Alvi [1] or the theoretical work of van Dommelen and Yapalparvi [2]. These are jets with a low level of injected mass flux, and are driven through a small orifice that is comparable

A. J. Williams (✉) · R. E. Hewitt
School of Mathematics, University of Manchester, Manchester M13 9PL, UK
e-mail: anthony.williams-2@manchester.ac.uk

in scale to the boundary-layer thickness. This approach to flow injection is different from the classical description of boundary layers affected by wall injection, which only consider injection over length scales that are significantly longer than the local boundary-layer thickness. Based upon the results of macro-scale injection, mass flux into the boundary layer through a surface is usually assumed to promote boundary-layer separation; see, for example, Catherall et al. [3]. Therefore, the ability of a micro-jet mechanism to inhibit separation in a boundary layer is somewhat counter intuitive, and the reason may lie in a fundamentally different response associated with short-scale spanwise forcing. When the boundary layer is forced over a sufficiently short spanwise length scale, it is necessary to re-introduce the effects of momentum diffusion in the spanwise direction. This leads to a slightly more complex dimensionless boundary-layer formulation:

$$\hat{U}\hat{U}_x + \hat{V}\hat{U}_Y + \hat{W}\hat{U}_Z = U_e(x)U_e'(x) + \hat{U}_{YY} + \hat{U}_{ZZ}, \tag{1a}$$

$$\hat{U}\hat{V}_x + \hat{V}\hat{V}_Y + \hat{W}\hat{V}_Z = -\hat{P}_Y + \hat{V}_{YY} + \hat{V}_{ZZ}, \tag{1b}$$

$$\hat{U}\hat{W}_x + \hat{V}\hat{W}_Y + \hat{W}\hat{W}_Z = -\hat{P}_Z + \hat{W}_{YY} + \hat{W}_{ZZ}, \tag{1c}$$

$$\hat{U}_x + \hat{V}_Y + \hat{W}_Z = 0, \tag{1d}$$

for a steady incompressible flow, where $\hat{V}$ is the velocity normal to the boundary and $\hat{W}$ is the spanwise velocity. Here (Y, Z) are scaled boundary-layer coordinates in the transverse and spanwise directions, respectively, and U_e is the (known) outer streamwise velocity such that $(\hat{U}, \hat{W}) \to (U_e(x), 0)$ as $Y \to \infty$; we will derive this system more formally in the next section. As for the classical boundary layer, the leading-order streamwise pressure gradient is determined by the free stream to be $-U_e(x)U_e'(x)$, but a three-dimensional approach requires the inclusion of a higher-order (unknown) pressure correction $\hat{P}$. This system is in essence a parabolised version of the Navier–Stokes equations, and as such can be marched downstream in x provided that there is no flow reversal of the streamwise velocity $\hat{U}$. This formulation has been considered before, for example, by Patankar and Spalding [4] and Patankar [5], in which (1) is referred to as 'three-dimensional parabolic flow'. The same system of equations also appears earlier in the work of Kemp [6] and was termed the 'boundary-region equations', a phrase that persists in the later literature, see, for example, the recent work of Goldstein et al. [7,8] or Ricco and Dilib [9].

The classical two-dimensional boundary-layer equations are simply recovered by seeking solutions of (1) with $W = 0$ (no cross flow) and no dependence on the spanwise coordinate Z. This approach leaves only (1a) and (1d) to determine the two-dimensional velocity field (U, V), whilst (1b) is a *decoupled* equation that allows one to subsequently determine $\hat{P}$. It is well known that this two-dimensional problem admits self-similar states for algebraically developing external flow speeds (that is, $U_e(x) = x^n$) in the form of the Falkner–Skan family of solutions:

$$Y = \left(\frac{2x^{1-n}}{n+1}\right)^{1/2} \eta, \tag{2a}$$

$$\hat{U}(x, Y) = x^n\, U(\eta), \quad \hat{V}(x, Y) = \left(\frac{(n+1)}{2x^{1-n}}\right)^{1/2} V(\eta). \tag{2b}$$

Using the change of variables

$$V = \frac{1-n}{n+1}\eta U - F(\eta), \tag{2c}$$

where $F(\eta)$ is a scaled streamfunction, the continuity equation (1d) becomes $U = F'(\eta)$, and the streamwise momentum equation (1a) reduces to the Falkner–Skan equation:

$$F''' + FF'' + \beta\left(1 - (F')^2\right) = 0, \tag{2d}$$

where $\beta = 2n/(n+1)$ is the Hartree parameter [10].

In the two-dimensional system, a self-similar wall injection is defined by the value of $F(0)$ (which is negative for injection), and a key phenomenon for the case of $n = 0$ (zero pressure gradient) is the so-called 'blow-off' event described by Kassoy [11]. In the absence of a pressure gradient, there is a critical (negative) value for $F(0)$,

at which the boundary-layer solution terminates (that is, it is 'blown off' the boundary). Upon approaching this value of the injection rate, the shear stress at the surface of the plate approaches zero, whilst the displacement of the boundary layer tends to infinity. The introduction of a positive pressure gradient ($n > 0$) into this same problem removes this singularity, and two-dimensional boundary-layer solutions continue to exist for all injection rates but with the increasing displacement as the injection rate increases. The relationship between the zero and non-zero pressure-gradient cases was clarified in a later paper by Kassoy [12] and also discussed in a non-interactive framework by Watson [13]. An obvious issue to address is the relevance of these classical (macro-scale) injection features to problems that involve micro-scale (Z-dependent) injection.

The recent work of Hewitt et al. [14] extended the classical two-dimensional formulation, in the absence of a pressure gradient (i.e. $n = 0$ such that $U_e = 1$), to a three-dimensional formulation by allowing injection over a spanwise length scale comparable to the boundary-layer thickness. This provides a new family of three-dimensional self-similar solutions to (1) that are analogues of (2) (albeit for $n = 0$) and driven by injection over short spanwise scales. Counter to the two-dimensional theory, Hewitt et al. showed that the resulting three-dimensional solutions continue to exist for injection velocities greater than the critical two-dimensional 'blow-off' injection rate. These new solutions take the form of low-speed streamwise-aligned streaks. These streak solutions were categorised into one of three regimes, where the geometry of the streak is determined by the injection rate and the width of the injection slot.

In this work, we again examine the effect of short-scale injection in the context of (1), with free-stream speeds of $U_e(x) = x^n$ and a focus on a favourable pressure gradient $n > 0$. Generalising the three-dimensional boundary-layer injection solutions of [14] to include an applied pressure gradient is important not only because non-uniform external flows are commonplace, but also because we know that for macro-scale injection, the flow character is significantly affected by the pressure gradient.

Although this work begins from (1), we subsequently make use of a transformed version of this system for the computational work that follows. Numerical calculations of the three-dimensional boundary-layer solutions are then presented; illustrative examples of both the zero and non-zero pressure-gradient cases will be shown for comparison. We demonstrate that a favourable pressure gradient significantly changes the flow response, largely eliminating the streamwise streaks found for uniform external flows. We also show that increasingly wide injection slots do not connect smoothly to the known results of the Falkner–Skan solutions when the pressure gradient parameter is below a critical value. Finally, we investigate the role of spatially unstable eigenmodes near to the centreline of the injection slot and relate these to the numerical results obtained for increasing injection-slot width.

2 Formulation

We consider a dimensional system of Cartesian coordinates (x^*, y^*, z^*) where x^* is increasing in the streamwise direction, y^* is the transverse coordinate and z^* is the spanwise coordinate. The corresponding velocity field is (u^*, v^*, w^*) and the pressure is p^*; in what follows an asterisk will be used for dimensional quantities. A flat plate defined by $y^* = 0$, $x^* > 0$ is aligned with the free-stream flow, $u^* = U_e^*(x^*)$, and the leading edge is located at $x^* = 0$ as shown in Fig. 1. We restrict attention to power-law external flows of Falkner–Skan type with $U_e^*(x^*) = U_\infty^*(x^*/L^*)^n$ where U_∞^* is a constant velocity scale, n is the constant pressure-gradient parameter and L^* is an arbitrary streamwise length scale. By defining a global Reynolds number via $Re = U_\infty^* L^*/\nu^*$, where ν^* is the constant kinematic viscosity of the fluid, we can introduce the corresponding boundary-layer expansions for $Re \gg 1$:

$$(x^*, y^*, z^*) = L^*(x, Re^{-1/2}Y, Re^{-1/2}Z), \tag{3a}$$

$$u^* = U_\infty^* \hat{U}(x, Y, Z) + \cdots, \tag{3b}$$

$$v^* = U_\infty^* Re^{-1/2} \hat{V}(x, Y, Z) + \cdots, \tag{3c}$$

$$w^* = U_\infty^* Re^{-1/2} \hat{W}(x, Y, Z) + \cdots, \tag{3d}$$

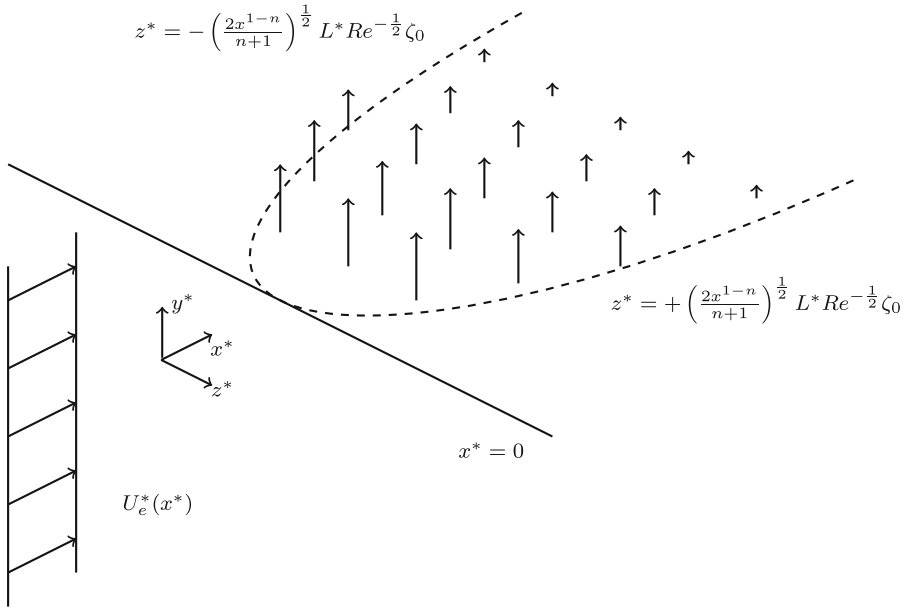

Fig. 1 A schematic representation of the flow domain; the leading edge of the flat plate is located at $x^* = 0$ and the plate is aligned with an oncoming power-law flow $U_e^*(x^*)$. An injection perpendicular to the surface of the plate $v^* = Re^{-1/2}\hat{V}_{\text{in}}$ is prescribed on $y^* = 0$ within the spanwise region specified by the dashed curve. The injection region grows downstream at the same rate as the boundary-layer thickness with ζ_0 specifying the relative width of the injection slot

$$p^* = \rho^* {U_\infty^*}^2 \left(-\tfrac{1}{2}U_e^2(x) + Re^{-1/2}p(x) + Re^{-1}\hat{P}(x, Y, Z) + \cdots\right), \tag{3e}$$

where ρ^* is the constant density and $U_e = x^n$ is the dimensionless free-stream speed. Substitution of (3) into the Navier–Stokes equations leads to the leading-order system of (1). It is worth highlighting that whilst $p(x)$ does not appear at leading order, the next correction $\hat{P}$ does.

At the surface of the plate, we impose no-slip boundary conditions $\hat{U} = \hat{W} = 0$ and an injection velocity $\hat{V} = \hat{V}_{\text{in}}(x, Z)$. It is this injection over the short spanwise scale (Z) that drives the three-dimensional response in the boundary layer. A computationally expensive approach to a discussion of (1) is to exploit the parabolicity in x and march downstream from an initial condition at the leading edge ($x = 0$), at each location solving for $(\hat{U}, \hat{V}, \hat{W}, \hat{P})$ in the plane spanned by (Z, Y). In this work, we will take a simpler approach, by looking for three-dimensional solutions that are self-similar in the downstream coordinate. Although this approach is clearly more restrictive, it allows us to clarify the mechanisms that dominate the flow response, in the hope that these same mechanisms still play a similar role in the more general (developing in x) flow.

Key to a self-similar solution is the new coordinate system

$$(Y, Z) = \left(\frac{2x^{1-n}}{n+1}\right)^{1/2} (\eta, \zeta)\,. \tag{4a}$$

This coordinate η is the usual Falkner–Skan similarity variable of (2a). To retain spanwise diffusion, at all downstream positions, we require that the spanwise lengthscale is always comparable to the transverse thickness of the layer, hence we employ the same form for ζ. For the velocity components, we seek a three-dimensional analogue of the standard solutions (2b):

$$\hat{U}(x, Y, Z) = x^n U(\eta, \zeta), \quad \left(\hat{V}(x, Y, Z), \hat{W}(x, Y, Z)\right) = \left(\frac{(n+1)}{2x^{1-n}}\right)^{1/2} (V(\eta, \zeta), W(\eta, \zeta))\,, \tag{4b}$$

where

$$V(\eta,\zeta) = \frac{1-n}{n+1}\eta U(\eta,\zeta) - \Phi(\eta,\zeta), \tag{4c}$$

$$W(\eta,\zeta) = \frac{1-n}{n+1}\zeta U(\eta,\zeta) - \Psi(\eta,\zeta). \tag{4d}$$

We apply (4) to the leading-order 'boundary-region equations' (1), but first it is convenient to cross differentiate (1b) and (1c) to eliminate the pressure correction $\hat{P}$. This cross differentiation naturally introduces a modified vorticity component; we will denote this vorticity by Θ, following the notation of Pal and Rubin [16]. At any x location, the similarity solution is determined over the cross-sectional (ζ,η) plane by finding the four unknowns (U,Φ,Ψ,Θ), which satisfy

$$(2-\beta)U = \Phi_\eta + \Psi_\zeta, \tag{5a}$$

$$\Theta = \Psi_\eta - \Phi_\zeta, \tag{5b}$$

and

$$\nabla^2 U = \beta\left[U^2 - 1\right] - \Phi U_\eta - \Psi U_\zeta, \tag{6a}$$

$$\nabla^2\Theta = 2(1-\beta)\left[\zeta U U_\eta - \eta U U_\zeta\right] - \Phi\Theta_\eta - \Psi\Theta_\zeta - (2-\beta)U\Theta, \tag{6b}$$

where ∇^2 is the two-dimensional Laplacian in the (ζ,η) plane. Despite being somewhat less intuitive than the primitive variable formulation, this form of (1) is well known in relation to corner boundary-layer flows, see for example the formulation of Dhanak and Duck [15] or Pal and Rubin [16].

We will follow the formulation of [15] further by combining (5a) and (5b) to obtain expressions for the Laplacian of both Φ and Ψ given by

$$\nabla^2\Phi = (2-\beta)U_\eta - \Theta_\zeta, \tag{6c}$$

$$\nabla^2\Psi = (2-\beta)U_\zeta + \Theta_\eta. \tag{6d}$$

This approach simplifies the numerical discretisation.

Our task is to solve (6) for (U,Ψ,Φ,Θ) in the (ζ,η) plane, at which point a three-dimensional solution is obtained at any point in the flow field via (4).

2.1 Boundary conditions

For consistency with the similarity form of the solution, we will restrict attention to injection distributions on the plate surface that are solely a function of the spanwise coordinate, such that

$$\hat{V}(x, Y=0, Z) = \hat{V}_{\text{in}}(x, Z) = V_{\text{in}}(\zeta). \tag{7}$$

If the injection is only over a finite range of ζ associated with the 'micro-slot', then the flow relaxes back to the usual two-dimensional solution (2) for $|\zeta| \gg 1$. For the injection profile $V_{\text{in}}(\zeta)$, we will focus our attention on the cases where the injection velocity is almost uniform in the slot region and decays rapidly outside this region. We therefore take the injection function to be

$$V_{\text{in}}(\zeta) = \frac{K}{2}\left[1 - \tanh\left(\gamma\left(|\zeta/\zeta_0| - 1\right)\right)\right], \tag{8}$$

where ζ_0 defines the spanwise extent of the slot region, γ determines the length scale of the transition from injection to no injection (we will take $\gamma = 20$ unless otherwise stated). The constant K defines the magnitude of the injection velocity with $K < 0$ indicating suction from the boundary layer and $K > 0$ indicating injection into the boundary layer. In what follows, we restrict our attention to the problem of injection only.

The surface boundary conditions arise from no-slip and the specified distribution of injection:

$$\Phi = -V_{\text{in}}(\zeta), \quad \Psi = U = 0, \quad \Theta = \Psi_\eta + V_{\text{in}\,\zeta} \quad \text{on} \quad \eta = 0. \tag{9a}$$

The contribution of $V_{\text{in}\,\zeta}$, the derivative of V_{in} with respect to ζ, arises from the definition of Θ given by (5b).

Assuming a reflectional symmetry about the $\zeta = 0$ centreline leads to

$$U_\zeta = \Phi_\zeta = \Psi = \Theta = 0 \quad \text{on} \quad \zeta = 0. \tag{9b}$$

Far away from the plate, we require $U \to 1$, $W \to 0$ in order to match to a free stream with no cross flow. This means that

$$U \to 1, \quad \Psi \to (1-\beta)\,\zeta \quad \text{and} \quad \Theta \to 0 \quad \text{as} \quad \eta \to \infty, \tag{9c}$$

where the condition on Θ is a vorticity decay constraint.

2.2 Numerical formulation

It is convenient to rescale the spanwise coordinate using the slot-width parameter, such that $\zeta = \zeta_0\hat{\zeta}$, and seek a nonlinear perturbation of the form

$$\Phi(\zeta,\eta) = \Phi_B(\eta) + \tilde{\Phi}(\hat{\zeta},\eta), \tag{10a}$$
$$\Psi(\zeta,\eta) = \zeta_0\hat{\zeta}\,\Psi_B(\eta) + \zeta_0\tilde{\Psi}(\hat{\zeta},\eta), \tag{10b}$$
$$U(\zeta,\eta) = U_B(\eta) + \tilde{U}(\hat{\zeta},\eta), \tag{10c}$$
$$\Theta(\zeta,\eta) = \zeta_0\hat{\zeta}\,\Theta_B(\eta) + \zeta_0\tilde{\Theta}(\hat{\zeta},\eta). \tag{10d}$$

Here the subscript 'B' terms represent the classical two-dimensional 'base flow' solution, whilst the tilde quantities are solely due to injection through the finite-width slot, which when combined give a three-dimensional solution (albeit one that is self-similar in the downstream coordinate). Therefore, if $K = 0$ (no injection), the 'B' terms remain, but the tilde quantities are all zero.

The classical two-dimensional solution (2) exists in the form $U_B = F'(\eta)$, $\Phi_B = F(\eta)$, $\Psi_B = (1-\beta)F'(\eta)$, $\Theta_B = (1-\beta)F''(\eta)$ where $F(\eta)$ satisfies (2d) subject to the boundary conditions $F(0) = F'(0) = 0$, $F'(\eta) \to 1$ as $\eta \to \infty$.

The nonlinear perturbation quantities are more difficult to determine, and are governed by

$$\hat{\nabla}^2\tilde{\Phi} = (2-\beta)\tilde{U}_\eta - \tilde{\Theta}_{\hat{\zeta}}, \tag{11a}$$
$$\hat{\nabla}^2\tilde{\Psi} = (2-\beta)\zeta_0^{-2}\tilde{U}_{\hat{\zeta}} + \tilde{\Theta}_\eta, \tag{11b}$$
$$\hat{\nabla}^2\tilde{U} = \beta\left[2U_B\tilde{U} + \tilde{U}^2\right] - \left(\hat{\zeta}\Psi_B + \tilde{\Psi}\right)\tilde{U}_{\hat{\zeta}} - \Phi_B\tilde{U}_\eta - \left(U_B' + \tilde{U}_\eta\right)\tilde{\Phi}, \tag{11c}$$
$$\begin{aligned}\hat{\nabla}^2\tilde{\Theta} = {} & 2(1-\beta)\left\{\hat{\zeta}\left(U_B + \tilde{U}\right)\tilde{U}_\eta + \hat{\zeta}U_B'\tilde{U} - \eta\zeta_0^{-2}\left(U_B + \tilde{U}\right)\tilde{U}_{\hat{\zeta}}\right\} \\ & - \left(\Phi_B + \tilde{\Phi}\right)\tilde{\Theta}_\eta - \hat{\zeta}\Theta_B'\tilde{\Phi} - \hat{\zeta}\Psi_B\tilde{\Theta}_{\hat{\zeta}} - \tilde{\Psi}\left(\Theta_B + \tilde{\Theta}_{\hat{\zeta}}\right) \\ & - (2-\beta)\left[\left(U_B + \tilde{U}\right)\tilde{\Theta} + \hat{\zeta}\Theta_B\tilde{U}\right],\end{aligned} \tag{11d}$$

where

$$\hat{\nabla}^2 \equiv \frac{\partial^2}{\partial \eta^2} + \frac{1}{\zeta_0^2}\frac{\partial^2}{\partial \hat{\zeta}^2}. \tag{11e}$$

The boundary conditions for the tilde quantities follow directly from (9a) and (9b).

Far from the injection region, we expect that the flow decays back towards the Falkner–Skan base solution. The decay of $(\tilde{\Phi}, \tilde{\Psi})$ is algebraic in the far field [19], and it is best to impose far-field boundary conditions that are consistent with this asymptotic decay. An explicit inclusion of this (relatively slow, algebraic) decay avoids the necessity for excessively large computational domains that otherwise arise with a simple zero Dirichlet conditions. Following this same approach for $\eta \gg 1$ at fixed $\hat{\zeta}$, we impose

$$\tilde{\Phi} \sim \frac{A\eta}{\eta^2 + \zeta_0^2\hat{\zeta}^2}, \quad \tilde{\Psi} \sim \frac{A\hat{\zeta}}{\eta^2 + \zeta_0^2\hat{\zeta}^2}, \quad \tilde{U} = \tilde{\Theta} = 0, \tag{12}$$

with corresponding conditions for $\hat{\zeta} \gg 1$ and $\eta = O(1)$ as discussed in [19]. The constant A is associated with a measure of the radial mass flux away from the injection region in the far field, with $A > 0$ being towards and $A < 0$ being away from the centreline ($\eta = \hat{\zeta} = 0$) of the injection slot.

Our computational scheme extends that of Hewitt et al. [14,19], to accommodate the non-zero pressure gradient in the free stream. We employ a non-uniform computational mesh that concentrates nodes in the slot region and at the edge of the slot. The governing equations and boundary conditions are approximated by second-order finite difference equations, and Newton iteration is used to determine the four unknowns: $(\tilde{\Phi}, \tilde{\Psi}, \tilde{U}, \tilde{\Theta})$ at each nodal location along with the mass flux coefficient A in (12). The resulting sparse linear system for the $4N_{\hat{\zeta}}N_\eta + 1$ unknowns, where $N_{\hat{\zeta}}$ and N_η are the numbers of nodes in the $\hat{\zeta}$ and η directions, respectively, is solved at each iteration using the Eigen library of Guennebaud et al. [20]. The computational domain is typically truncated at $\hat{\zeta} = \hat{\zeta}_\infty = 16$, $\eta = \eta_\infty = 128$ with $N_{\hat{\zeta}} = N_\eta = 401$, i.e. approximately 6.4×10^5 degrees of freedom. The results presented below are verified for convergence and are not dependent upon these choices of mesh size or domain size.

3 Results: three-dimensional injection states

When there is no injection through the surface of the plate, $K = 0$, the Falkner–Skan solution given by (2) is recovered and the flow remains two-dimensional throughout the domain. However, any non-zero injection through the plate surface over a finite spanwise extent ζ_0 generates a three-dimensional deviation from the two-dimensional base flow in this neighbourhood. We present results for $K > 0$ (injection) and $0 \leq n < 1$, corresponding to $0 \leq \beta < 1$; when sufficiently far from the injection slot, such that the injection effects are small, $\beta = 0$ leads to a Blasius flow whilst $\beta \to 1$ leads to a Hiemenz flow. In this range of pressure gradients, the boundary-layer thickness increases downstream from the leading edge.

The previous work of [14] showed that for $K > 0$ (injection) and no applied pressure gradient ($\beta = 0$), three distinct flow regimes are observed, as the injection-slot width ζ_0 is increased. These three regimes are delineated by the injection rates: $0 < K < K_I \approx 0.876$, $K_I < K < K_{II} \approx 1.95$ and $K > K_{II}$. The left-hand column of Fig. 2 shows the three flow regimes present when $\beta = 0$. In the weak injection regime (a) $0 < K < K_I$, although a three-dimensional state is obtained, the solution remains qualitatively similar to the underlying Blasius solution with a weak spanwise variation. Near to the centreline $\hat{\zeta} = 0$, there is a slight thickening of the boundary layer, but the injection flow does not have a significant impact on the solution. Upon increasing the injection amplitude such that $K_I < K < K_{II}$, a low-speed streak develops in the injection region $\hat{\zeta} < 1$. In this moderate injection regime (c), a displaced shear layer separates the low streamwise speeds inside the streak from the high-speed outer flow. The size of this streak remains confined to lie within the slot region (i.e. $\zeta < \zeta_0$). In the strong injection regime

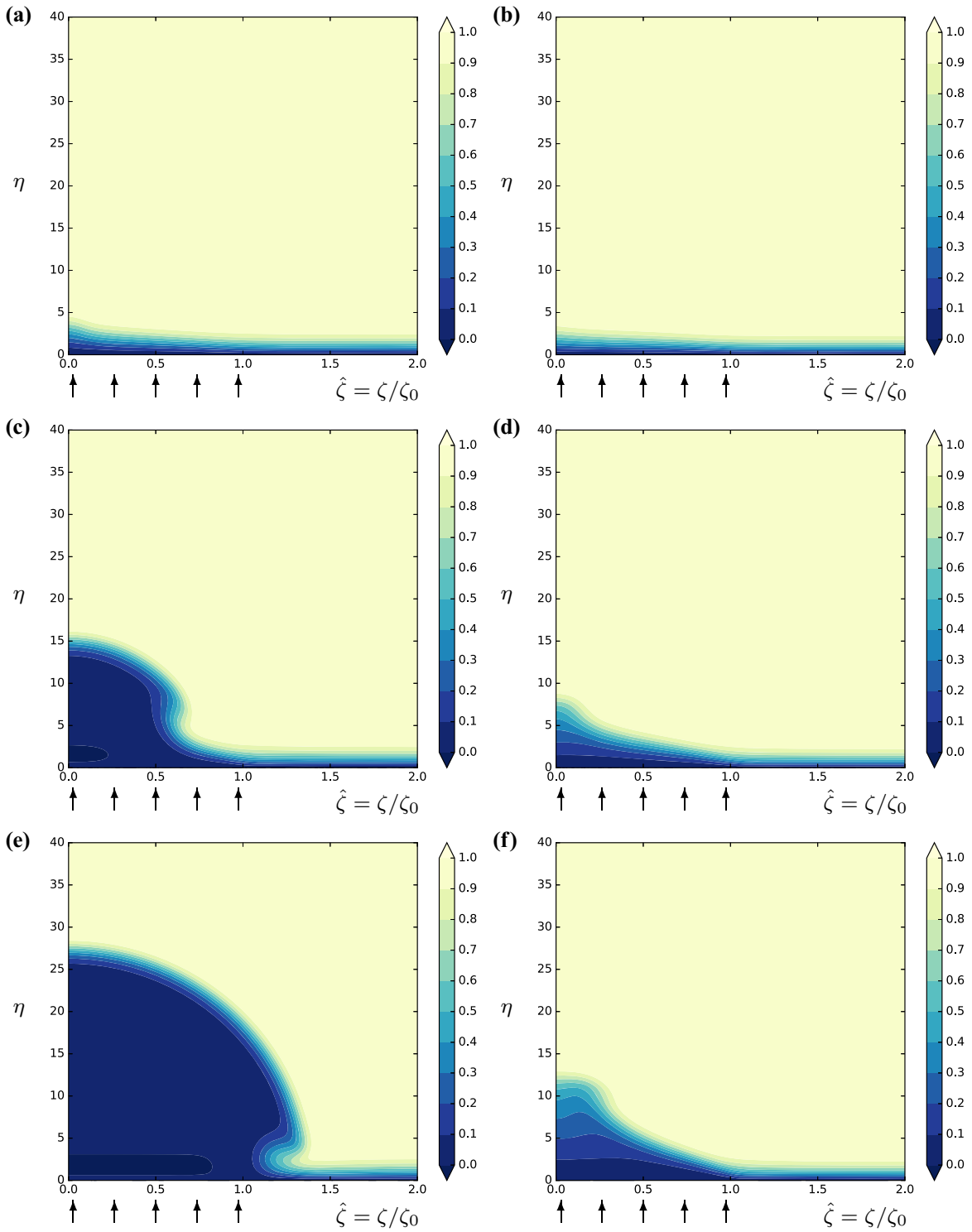

Fig. 2 The *left-hand* and *right-hand* columns show contours of streamwise velocity U for $\beta = 0$ and $\beta = 0.1$, respectively. Injection rates increase down the page such that for **a**, **b** $K = 0.5$, **c**, **d** $K = 1.5$ and **e**, **f** $K = 2.5$. The injection through the plate surface is concentrated in the region $|\zeta| < \zeta_0$ as defined by (8) and indicated by the arrows, whilst $\zeta = 0$ is a symmetry line. For $\beta = 0$ (**a**, **c**, **e**) three distinct flow regimes are observed as described in [14]. However results for $\beta = 0.1$ (**b**, **d**, **f**) show a qualitatively different response

(e) $K > K_{II}$, a much more prominent low-speed streak is observed which is separated from the outer flow by a semi-circular free shear layer. Due to the low streamwise velocity inside the streak, the mass injected into the layer through the plate must be ejected through the shear layer, and this constraint allows one to predict the streak radius as ζ_0 increases [14].

In the presence of a favourable pressure gradient ($\beta > 0$), Fig. 2b, d, f, we do not see the three distinct types of flow (as found for $\beta = 0$) with their prominent low-speed streaks. The introduction of a non-zero pressure gradient, as shown in the right-hand column of Fig. 2 (with $\beta = 0.1$), significantly alters the streamwise velocity U in the neighbourhood of the slot ($|\zeta| < \zeta_0$). The two-dimensional Falkner–Skan solution that exists far away from the injection slot ($\hat{\zeta} \gg 1$) is modified in the injection region to a much lesser degree for $\beta > 0$. There is no obvious semi-circular low-speed region as shown by comparison of Fig. 2e for $\beta = 0$ and Fig. 2f for $\beta = 0.1$. In general, injection leads to a thickening of the near-plate layer, which is to be expected.

Instead, we obtain a much less dramatic flow response, but one that nonetheless has two distinct properties: we either find that at fixed $K > 0$ (injection) and $\beta > 0$ (i) the solution near the centreline becomes increasingly displaced from the plate as ζ_0 increases or (ii) the low-speed region in the slot region $\zeta < \zeta_0$ remains largely unaffected as the slot width is increased. This behaviour is seen in Fig. 3a, b where contours are shown for $K = 4$, $\beta = 0.2$ and $\zeta_0 = 20$ in (a) and for $\zeta_0 = 40$ in (b). However, this growing η scale is not observed in all cases, as demonstrated by Fig. 3c, d in the case $K = 4$, $\beta = 0.8$, $\zeta_0 = 20$ in (c) and $\zeta_0 = 40$ in (d). We will return to explain this feature in the subsequent analysis below, to identify how the choices of β and K determine the observed behaviour.

Comparing these results to the zero pressure-case ($\beta = 0$) we find that a favourable pressure gradient acts to inhibit (although not eliminate entirely) the rapid displacement of a low-speed layer from the plate surface. The greatly reduced extent of the low-speed streak indicates an increase in the streamwise mass flux and therefore a reduced radial flow into the far field, compared with the zero pressure-gradient case. This reduction in the radial mass flux is reflected in a reduction in the magnitude of the mass flux parameter A contained in (12). Again, we return to validate this feature via asymptotic methods below.

4 Asymptotic description for $\zeta_0 \to \infty$: the macro-scale slot limit

An asymptotic description of the flow in the limit of a large injection-slot width, $\zeta_0 \to \infty$, is presented below. When $0 < \beta < 1$ a large aspect ratio viscous layer is present, spanned by $\eta = O(1)$ and $\zeta = O(\zeta_0)$ for all values of $K > 0$. To describe the flow, we use the rescaled coordinate $\hat{\zeta} = \zeta/\zeta_0$ and

$$U(\zeta, \eta; \zeta_0) = U_0(\hat{\zeta}, \eta) + \cdots, \tag{13a}$$

$$\Phi(\zeta, \eta; \zeta_0) = \Phi_0(\hat{\zeta}, \eta) + \cdots, \tag{13b}$$

$$\Psi(\zeta, \eta; \zeta_0) = \zeta_0 \hat{\zeta} \Psi_0(\hat{\zeta}, \eta) + \cdots, \tag{13c}$$

$$\Theta(\zeta, \eta; \zeta_0) = \zeta_0 \hat{\zeta} \Theta_0(\hat{\zeta}, \eta) + \cdots. \tag{13d}$$

Using (13) and taking the limit $\zeta_0 \to \infty$, we find that at leading order, (6) reduces to

$$(2 - \beta) U_0 = \Phi_{0\eta} + \hat{\zeta} \Psi_{0\hat{\zeta}} + \Psi_0, \tag{14a}$$

$$\Theta_0 = \Psi_{0\eta}, \tag{14b}$$

$$U_{0\eta\eta} = \beta \left[U_0^2 - 1 \right] - \Phi_0 U_{0\eta} - \hat{\zeta} \Psi_0 U_{0\hat{\zeta}}, \tag{14c}$$

$$\Theta_{0\eta\eta} = 2(1 - \beta) U_0 U_{0\eta} - \Phi_0 \Theta_{0\eta} - \Psi_0 \Theta_0 - \hat{\zeta} \Psi_0 \Theta_{0\hat{\zeta}} - (2 - \beta) U_0 \Theta_0. \tag{14d}$$

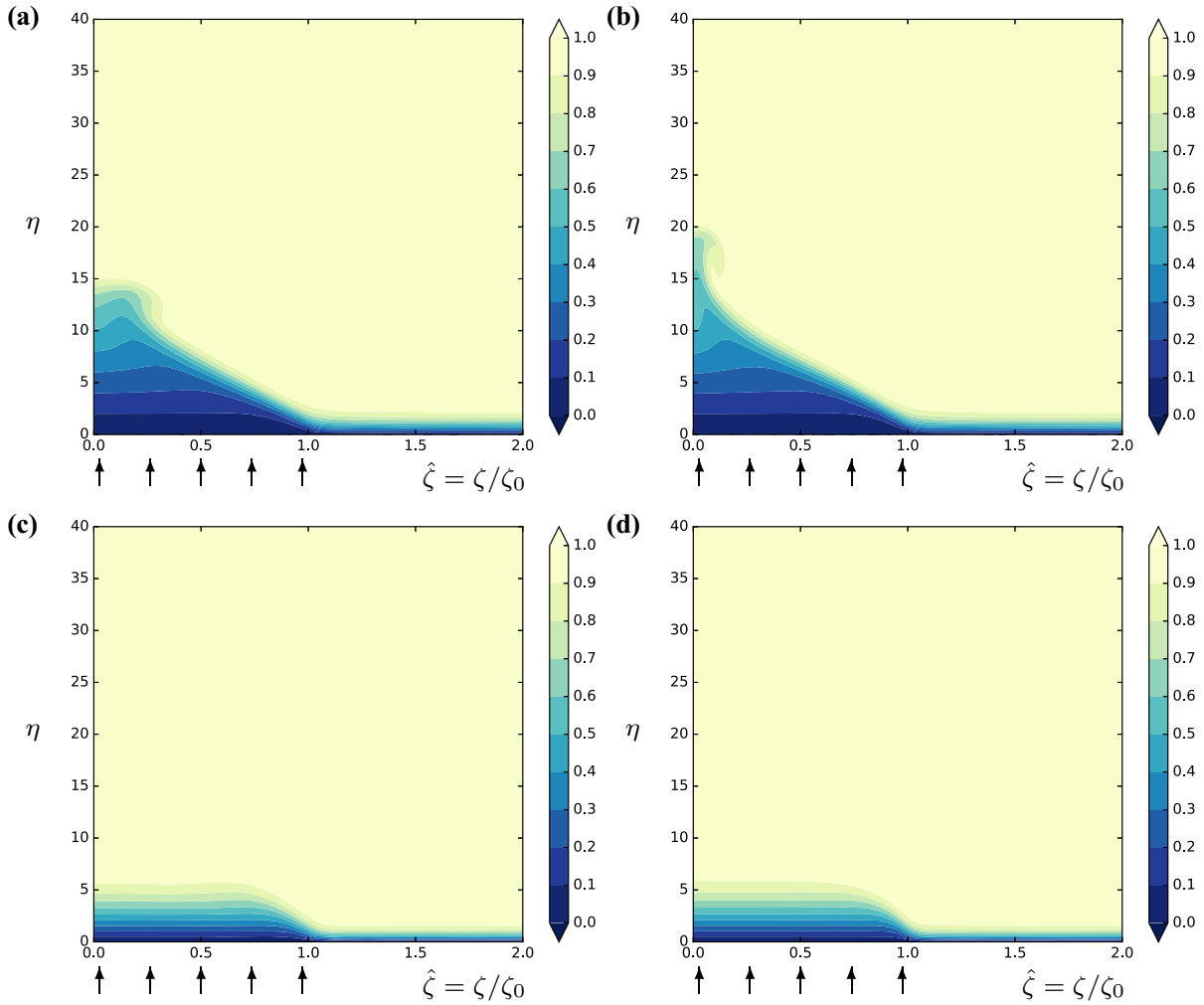

Fig. 3 Contours of the streamwise velocity U are shown for injection rate $K = 4$ and pressure gradients **a**, **b** $\beta = 0.2$ and **c**, **d** $\beta = 0.8$. Injection through the boundary is confined to the region $|\zeta| < \zeta_0$, as indicated by the *arrows*. The *left-hand* column is for an injection-slot width of $\zeta_0 = 20$ and the *right-hand* column is for $\zeta_0 = 40$. For $\beta = 0.2$ (**a**, **b**), an increasing injection-slot width ζ_0 leads to a growing η scale and eruptive behaviour near to $\zeta = 0$. For $\beta = 0.8$ (**c**, **d**), this growing η scale is not observed for increasing ζ_0 with a benign response seen near to $\zeta = 0$

This system is parabolic in $\hat{\zeta}$ and the 'windward' direction is determined by the sign of Ψ_0. If $\Psi_0 > 0$ for all $\eta > 0$ then the far-field solution can be extended from $\hat{\zeta} \gg 1$ (where the flow is know to be the classical Falkner–Skan solution) towards $\hat{\zeta} = 0$ by parabolic marching, subject to the conditions

$$U_0 = \Psi_0 = 0, \quad \Phi_0 = -V_{\text{in}} \quad \text{on} \quad \eta = 0, \tag{14e}$$

$$U_0 \to 1, \quad \Theta_0 \to 0, \quad \Psi_0 \to 1 - \beta \quad \text{as} \quad \eta \to \infty, \tag{14f}$$

where V_{in} is defined by (8).

In the far-field $\hat{\zeta} \gg 1$, the 'initial' state for (14) is the Falkner–Skan solution, for which $\Psi_0 = (1 - \beta)U_0$, which means that there is no cross flow so $W = 0$ in (4d). If we start (14) from a state with no cross flow, then it retains this feature for all subsequent $\hat{\zeta}$, and hence the system (14) can be reduced to a simpler form

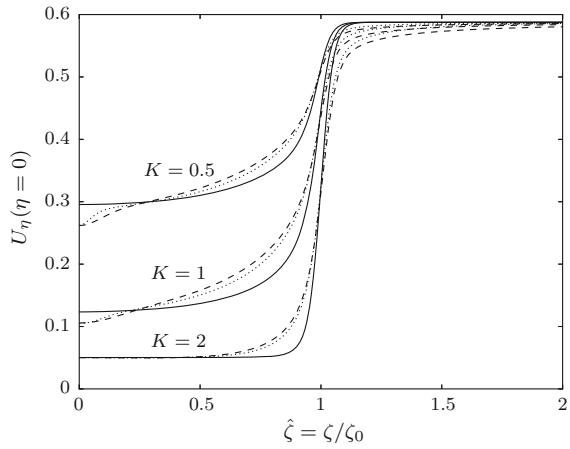

Fig. 4 The shear distribution at the plate surface $U_\eta(\hat{\zeta}, \eta = 0)$, near to the injection region, for various blowing intensities K with the pressure gradient $\beta = 0.1$. The *dashed lines* are for $\zeta_0 = 20$, and the *dotted lines* are for $\zeta_0 = 40$; the *solid line* depicts the shear distribution predicted by the parabolic system (15)

$$U_0 = \Phi_{0\eta} + (1-\beta)\hat{\zeta} U_{0\hat{\zeta}}, \tag{15a}$$

$$U_{0\eta\eta} = \beta\left[U_0^2 - 1\right] - \Phi_0 U_{0\eta} - (1-\beta)\hat{\zeta} U_0 U_{0\hat{\zeta}}, \tag{15b}$$

with $U_0 = 0$, $\Phi_0 = -V_{\text{in}}$ on $\eta = 0$ and $U_0 \to 1$ as $\eta \to \infty$. We may also note that setting $\hat{\zeta} = 0$, under the assumption that $\hat{\zeta}$ derivatives can then be neglected in this limit, reproduces the Falkner–Skan equation (2d), but subject to an injection at the surface of $V_{\text{in}}(\hat{\zeta} = 0) = K$. This suggests that for sufficiently large slot widths, we may eventually recover the classical Falkner–Skan solution at the centreline of the injection region. However, this is not always true, and as we shall see in the next section, small amounts of residual cross flow can dominate for small $\hat{\zeta}$, leading to rather different behaviours in some cases. Nevertheless, we begin by assuming that such cross flow is small and that (15) is sufficient to describe the flow.

When $\beta = 0$ solutions to (2d) only exist for $K \lesssim 0.876$. Marching of (15) for $K \gtrsim 0.876$ leads to a singular response at a finite value of $\hat{\zeta} > 0$ because the wall shear stress $U_{0\eta}(\eta = 0)$ becomes equal to zero; this is associated with a change in the 'windward' direction of the parabolic system. When $\beta > 0$, marching of (15) to $\hat{\zeta} = 0$ can be achieved for *all* values K. It is the presence of this singularity (when $\beta = 0$) that leads to the other types of low-speed streaks described by Hewitt et al. [14].

The behaviour of the downstream shear is illustrated in Fig. 4. When $\beta \neq 0$ we can see that the wall shear stress never reaches zero and instead approaches a finite value as $\hat{\zeta} \to 0$. For large injection rates K, we find that the wall shear $U_\eta(\eta = 0) \sim \beta/K$ in the injection region thus agreeing with the two-dimensional theory of Kubota and Fernandez [21].

For large η, the vertical velocity component in the parabolic solution is of the form

$$\Phi_0 \sim \eta + \delta_F + \delta_{\text{in}}(\hat{\zeta}). \tag{16}$$

Here δ_F is the constant displacement thickness associated with the Falkner–Skan solution for flow on a flat plate in the absence of injection. We also have a displacement $\delta_{\text{in}}(\hat{\zeta})$ which is varying in the spanwise direction due to the wall injection over a finite spanwise region. If there is no injection though the plate surface then $\delta_{\text{in}} \equiv 0$ for all $\hat{\zeta}$ and there is no $\hat{\zeta}$-dependent perturbation to the Falkner–Skan solution, however in general $\delta_{\text{in}}(\hat{\zeta})$ is non-zero and must be taken into consideration.

We now consider the inviscid region defined by $\eta = \zeta_0\hat{\eta}$ and $\zeta = \zeta_0\hat{\zeta}$. In this outer region, we may rewrite the vertical velocity component as

$$\Phi(\zeta, \eta) = \zeta_0\hat{\eta} + \delta_F + \phi(\hat{\zeta}, \hat{\eta}), \tag{17}$$

where $\phi = O(1)$ in order to match with the spanwise varying displacement induced by the parabolic solution (15) and $\zeta_0\hat{\eta} + \delta_F$ is the (outer) $\eta \to \infty$ limit of the (inner) Falkner–Skan solution. Rewriting (5a) and (5b) in terms of $\hat{\zeta}$ and $\hat{\eta}$, and since both U and Θ remain $o(\zeta_0^{-2})$, we find that ϕ is determined by the harmonic problem,

$$\hat{\nabla}^2\phi = 0, \tag{18a}$$

subject to

$$\phi(\hat{\zeta}, \hat{\eta} = 0) = \delta_{\text{in}}(\hat{\zeta}). \tag{18b}$$

Here $\delta_{\text{in}}(\hat{\zeta})$ is determined by the solution of the parabolic system (15). It is also possible to obtain a similar Laplace problem for the corresponding Ψ velocity perturbation $\psi(\hat{\zeta}, \hat{\eta})$. The solution to the problem (18) is obtained using a Green's function approach

$$\phi(\hat{\zeta}, \hat{\eta}) = \frac{1}{\pi}\int_{z=-\infty}^{+\infty} \frac{\delta_{\text{in}}(z)\hat{\eta}}{\hat{\eta}^2 + (\hat{\zeta} - z)^2}\mathrm{d}z. \tag{19}$$

We know from (12) that in the far field

$$\phi \sim \frac{\hat{A}\hat{\eta}}{\hat{\zeta}^2 + \hat{\eta}^2}, \tag{20}$$

where $A = \zeta_0\hat{A}$. Given this far-field behaviour, the total radial mass flux due to the spanwise variation at the edge of the boundary layer is $\hat{A}\zeta_0\pi = A\pi$. On the other hand, the flux from the inner parabolic region induced by the injection is $M\zeta_0$ where

$$M = \int_{-\infty}^{+\infty} \delta_{\text{in}}(\hat{\zeta})\mathrm{d}\hat{\zeta}. \tag{21}$$

Combining these two expressions for the mass flux gives

$$A = \frac{M\zeta_0}{\pi}, \tag{22}$$

so the mass flux coefficient A is proportional to the blowing width ζ_0 and the integral of the spanwise varying displacement. The description provided by (22) applies to the $\beta = 0$ case of [14], but the difference here lies in the mass flux integral being a function of the pressure-gradient parameter, $M = M(\beta)$.

This asymptotic description suggests that, for large injection slot widths $\zeta_0 \gg 1$ and $\beta > 0$, the mass flux coefficient A remains linearly dependent upon ζ_0 for any fixed $K > 0$. This is markedly different to when $\beta = 0$, in which case increased injection ($K \gtrsim 1.95$) leads to a mass flux coefficient A that is proportional to ζ_0^2 and the formation of a low-speed semi-circular 'bubble'.

Computation of $\delta_{\text{in}}(\hat{\zeta})$ by parabolic marching of (15), allows one to determine $M(\beta)$ via the integral (21). In Fig. 5, we show the asymptotic prediction (22) for a range of values of $\beta = 0.05, 0.1, 0.4, 0.8$, which effectively shows the reduction in radial mass flux in the (ζ, η) plane as the pressure gradient is increased. The same figure also shows numerically determined values of A, as obtained from (6), in the particular case $\beta = 0.1$ and increasing injection-slot widths $\zeta_0 = 2, 4$ and 8. The linear relationship between the mass flux coefficient A and the injection width ζ_0 is confirmed with good agreement between the numerically determined values and the asymptotic prediction for the representative value of $\beta = 0.1$.

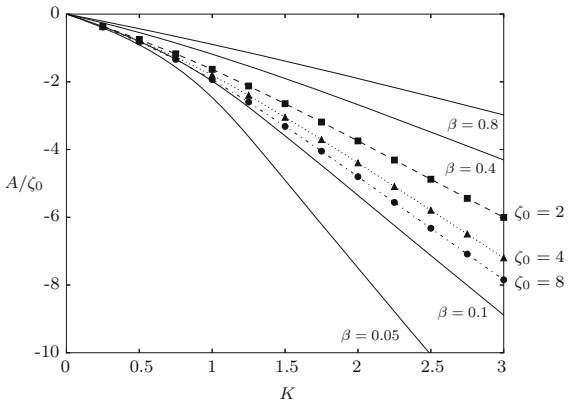

Fig. 5 The *solid lines* show the asymptotic prediction $A/\zeta_0 \sim M/\pi$ for large ζ_0, as determined from the parabolic system (15) and (21) for $\beta = 0.05, 0.1, 0.4, 0.8$. The data points show values of A/ζ_0 for increasing injection rates K and $\beta = 0.1$, as determined numerically from the governing equations (6) for increasing injection-slot widths $\zeta_0 = 2$, 4 and 8

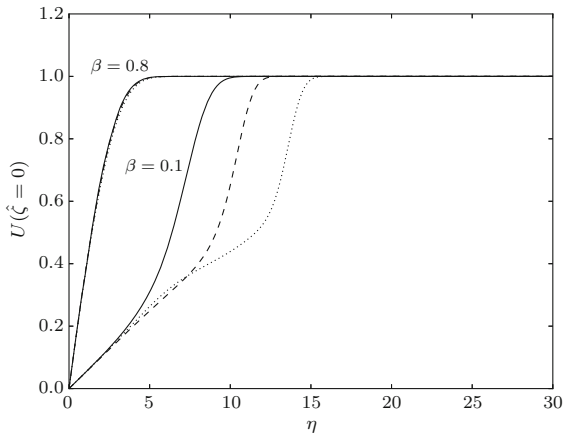

Fig. 6 Streamwise velocity U profiles at the centreline of the injection region $\hat{\zeta} = 0$ for $K = 2$ along with a small favourable pressure gradient, $\beta = 0.1$, and a larger favourable pressure gradient $\beta = 0.8$. For each value of β, the solid line shows the Falkner–Skan solution with injection as predicted by (15), the *dashed* and *dotted lines* show the solution of (6) for $\zeta_0 = 20$ and 40, respectively

The leading-order parabolic solution of (15) captures the full numerical solution for $\hat{\zeta} = O(1)$, as evidenced by the results of Figs. 4 and 5, but there are some additional features that it does not describe. One feature is the influence of spanwise diffusion around the edge of the injection slot, although this region is small compared to the $\hat{\zeta} = O(1)$ scale. A more important issue is the behaviour shown in Fig. 3. For some choices of β and K, we find an increasing boundary-layer thickness local to the centreline of the slot as ζ_0 increases. We now examine the role of cross-flow eigenmodes to the parabolic system (15), which allows us to determine a critical favourable pressure gradient beyond which this thickening local to the centreline is not found.

5 Three-dimensional eigenmodes for $\hat{\zeta} \ll 1$

In Fig. 6, we show the streamwise velocity profiles as measured on the centreline of the injection slot ($\hat{\zeta} = 0$) for $K = 2$, $\beta = 0.1, 0.8$ and $\zeta_0 = 20, 40$. When $\beta = 0.8$ the parabolic solution (15), in the limit of $\hat{\zeta} \to 0$, is in agreement with the numerical solution of the full equations (6) for both $\zeta_0 = 20$ and $\zeta_0 = 40$. On the other hand, when $\beta = 0.1$ the parabolic solution and the full solution only agree near to $\eta = 0$ and for large η, whilst at intermediate values of η there is a large discrepancy. Furthermore, increasing the slot width (ζ_0) only exacerbates the difference. This reinforces the picture of the flow response presented by Fig. 3, which similarly shows a benign dependence on ζ_0 when $\beta = 0.8$ compared to the eruptive behaviour found for $\beta = 0.2$. This deviation from the behaviour predicted by the parabolic solution is confined to near the centreline $\hat{\zeta} \ll 1$ and as such it is necessary to alter our approach in this region. It is clear that, as the slot is widened, some pressure gradients result in a centreline flow that is consistent with the corresponding injection-affected Falkner–Skan solution, but some instead result in what appears to be an increasing eruptive behaviour in this region.

In order to understand the behaviour near to $\hat{\zeta} = 0$, we seek to describe the spatial evolution of a small perturbation to the parabolic solution of the previous section. To perform this, we expand in the form

$$U = U_0(\hat{\zeta}, \eta) + \epsilon u(\hat{\zeta}, \eta), \tag{23a}$$

$$\Phi = \Phi_0(\hat{\zeta}, \eta) + \epsilon\varphi(\hat{\zeta}, \eta), \tag{23b}$$

$$\Psi = \zeta_0\hat{\zeta}\left(\Psi_0(\hat{\zeta}, \eta) + \epsilon\psi(\hat{\zeta}, \eta)\right), \tag{23c}$$

$$\Theta = \zeta_0\hat{\zeta}\left(\Theta_0(\hat{\zeta}, \eta) + \epsilon\vartheta(\hat{\zeta}, \eta)\right). \tag{23d}$$

Setting $\epsilon = 0$ we recover the leading-order system (14), which if started from a state with no cross flow, has a solution with $\Psi_0 = (1-\beta)U_0$, which leads to the simpler form (15). For $\epsilon \ll 1$, the linearised system for $(u, \varphi, \psi, \vartheta)$ is given by

$$(2-\beta)u = \varphi_\eta + \psi + \hat{\zeta}\psi_{\hat{\zeta}}, \tag{24a}$$

$$\vartheta = \psi_\eta, \tag{24b}$$

$$u_{\eta\eta} = 2\beta U_0 u - \Phi_0 u_\eta - U_{0\eta}\varphi - \hat{\zeta}\left(U_{0\hat{\zeta}}\psi + \Psi_0 u_{\hat{\zeta}}\right), \tag{24c}$$

$$\begin{aligned}\vartheta_{\eta\eta} = {} & 2(1-\beta)\left[U_{0\eta}u + U_0 u_\eta\right] - \Theta_{0\eta}\varphi - \Phi_0\vartheta_\eta - \Psi_0\left(\vartheta + \hat{\zeta}\vartheta_{\hat{\zeta}}\right) \\ & - \left(\Theta_0 + \hat{\zeta}\Theta_{0\hat{\zeta}}\right)\psi - (2-\beta)\left(U_0\vartheta + \Theta_0 u\right).\end{aligned} \tag{24d}$$

For $\hat{\zeta} \ll 1$, solutions to these $O(\epsilon)$ perturbation equations exist in the form

$$\left(u(\hat{\zeta}, \eta), \varphi(\hat{\zeta}, \eta), \psi(\hat{\zeta}, \eta), \vartheta(\hat{\zeta}, \eta)\right) = \hat{\zeta}^\lambda\left(u_0(\eta), \varphi_0(\eta), \psi_0(\eta), \vartheta_0(\eta)\right). \tag{25}$$

The $O(\epsilon^0)$ system merely reduces to the Falkner–Skan equation (2d) with an injection boundary condition such that $U_0 = F'(\eta)$, $\Phi_0 = F(\eta)$, $\Psi_0 = (1-\beta)F'(\eta)$, $\Theta_0 = (1-\beta)F''(\eta)$ and $F(0) = -K$, along with the other usual boundary conditions. The $O(\epsilon)$ system, with the local form (25) leads to an eigenvalue problem

$$(2-\beta)u_0 - \varphi_0' - \psi_0 = \lambda\psi_0, \tag{26a}$$

$$\vartheta_0 - \psi_0' = 0, \tag{26b}$$

$$u_0'' - 2\beta U_0 u_0 + \Phi_0 u_0' + U_{0\eta}\varphi_0 = -\lambda\Psi_0 u_0, \tag{26c}$$

$$\begin{aligned}\vartheta_0'' - {} & 2(1-\beta)\left[U_{0\eta}u_0 + U_0 u_0'\right] + \Theta_{0\eta}\varphi_0 + \Phi_0\vartheta_0' + \Psi_0\vartheta_0 + \Theta_0\psi_0 \\ & + (2-\beta)(U_0\vartheta_0 + \Theta_0 u_0) = -\lambda\Psi_0\vartheta_0,\end{aligned} \tag{26d}$$

where the prime notation is used to denote derivatives with respect to η. The homogeneous boundary conditions to be imposed are $u_0(0) = \varphi_0(0) = \psi_0(0) = 0$ and $u_0, \psi_0, \vartheta_0 \to 0$ as $\eta \to \infty$. Here $\lambda = \lambda_r + i\lambda_i$ is a complex eigenvalue which we must determine, to describe the spatial behaviour of the perturbation on approaching the slot centreline. If the real part of the eigenvalue is negative ($\lambda_r < 0$) as $\hat{\zeta} \to 0$ then the perturbation grows and the corresponding eigenmode is linearly unstable. In such cases, we should not expect, in general, to recover a Falkner–Skan solution near $\hat{\zeta} = 0$.

Using a standard central differencing scheme, we may discretise (26) producing a generalised eigenvalue problem of the form $A\mathbf{v}_n = \lambda_n B\mathbf{v}_n$ where A and B are $6N_\eta \times 6N_\eta$ matrices and $n \in \{1, \ldots, 6N_\eta\}$. Performing a generalised Schur decomposition to factorise A and B, we are able to find values of λ_n which are numerical approximations to the eigenvalue spectrum of (26).

Figure 7a shows the real part of the most relevant eigenvalue for various values of the 'injection' parameter K with $\beta = 0.1, 0.2, 0.4, 0.5, 0.6$. For a more complete picture, the figure covers $K \in [-2, 3]$ with $K < 0$ indicating suction and $K > 0$ injection. The most relevant eigenvalue in this case is the one with the smallest real part, and in Fig. 7a, the eigenvalues shown are all purely real with $\lambda_i = 0$.

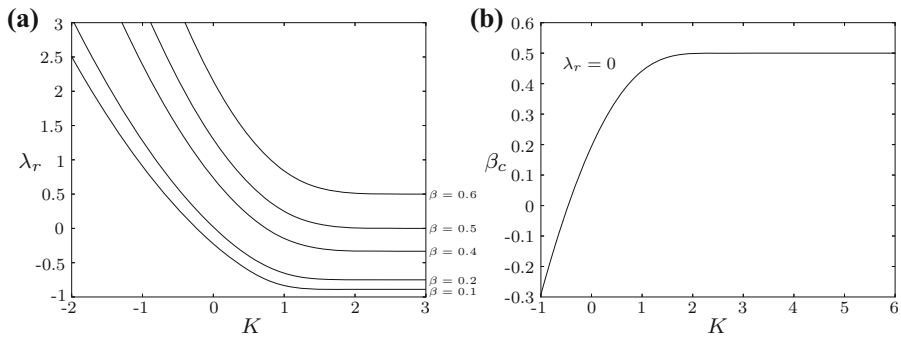

Fig. 7 **a** The real part of the eigenvalues $\lambda = \lambda_r + i\lambda_i$ for perturbations to the parabolic system (15) as $\hat{\zeta} \to 0$. The eigenvalues are found from the solution of (26) for injection magnitudes $K \in [-2, 3]$ and pressure gradients $\beta = 0.1, 0.2, 0.4, 0.5, 0.6$. Only the smallest eigenvalues are shown for each of the values of β as all the other eigenvalues remain positive regardless of the value of K. **b** The critical pressure gradient $\beta_c(K)$ at which $\lambda_r = 0$ for $K \in [-1, 6]$

When $\beta = 0.1$ (for example) the smallest eigenvalue is positive when K is sufficiently negative (suction) but as K increases the real part of the eigenvalue becomes negative, $\lambda_r < 0$, and approaches a constant negative value for large K (strong injection). With $\lambda_r < 0$ this eigenmode will come to dominate the solution as $|\hat{\zeta}| \to 0$, and when sufficiently close to the centreline of the injection slot one must appeal to the re-inclusion of spanwise diffusion and/or nonlinear effects to regularise this linear spatial growth. The eigenfunction of this spatial mode is such that there is a non-zero cross-flow velocity associated with the perturbation, that is $W \neq 0$ as defined by (4d).

Figure 7a demonstrates the impact of increasing the pressure gradient on the spatial stability of the solution near to $\hat{\zeta} = 0$. As the value of β increases, λ_r typically increases until at a critical value $\beta_c(K)$ the eigenvalue with the smallest real part has $\lambda_r \geq 0$. This means that only for $\beta \geq \beta_c(K)$ can we expect to recover the Falkner–Skan solution for $|\hat{\zeta}| \ll 1$ if there are perturbations with non-zero cross flow.

Figure 7b shows the functional relationship between injection and the pressure gradient parameter, such that there exists a spatially neutral mode with $\lambda_r = 0$; as such this represents a neutral curve above which we expect a benign response near to $\hat{\zeta} = 0$ and below which we expect the solution to be affected by these centreline eigenmodes. As seen in Fig. 7a, the eigenvalue approaches a constant value for sufficiently large $K > 0$ (strong injection). Therefore, we expect β_c to also asymptote to a constant as K increases. As shown in Fig. 7b, the numerical evidence suggests that $\beta_c \approx 1/2$ for large $K > 0$, although we have not sought to demonstrate this explicitly via an asymptotic analysis.

6 Discussion

Three-dimensional similarity solutions have been presented for laminar flow of velocity $O(U_\infty^* x^n)$ over a flat plate, driven by a favourable pressure gradient that is parametrised by n in the usual Falkner–Skan approach. The three dimensionality is driven by injection over the short spanwise scale of width $O\left(\zeta_0 Re^{-1/2} x^{(1-n)/2} L^*\right)$. The injection velocity is weak, $O\left(K Re^{-1/2} x^{(n-1)/2}\right)$, where x is a dimensionless streamwise coordinate and Re a Reynolds number based on the streamwise length scale L^*. The above choices for the slot and injection velocity scaling mean that the slot width is always a constant ratio of the boundary-layer thickness at all downstream locations. This approach allows for solutions that are self-similar in the downstream x coordinate, being three-dimensional extensions of the Falkner–Skan solution. In general, this need not be the case, and the approach can be generalised to parabolic marching in the downstream direction to account for other choices. Away from the injection slot, at large spanwise distances, the flow returns back to the classical two-dimensional Falkner–Skan profile appropriate for an impermeable boundary.

In the absence of a free-stream pressure gradient (that is $\beta = 0$, where β is the Hartree parameter), the earlier work of Hewitt et al. [14] has shown that an increasing injection-slot width (ζ_0) leads to one of three flow regimes.

Selection between these three regimes depends upon the size of the injection velocity which is parametrised by K. The two critical values of $K > 0$ that separate the three regimes are $K = K_I \approx 0.876$ and $K = K_{II} \approx 1.95$. The three flow regimes are exemplified by the streamwise velocity contours shown in the left hand column of Fig. 2. However, in the presence of a favourable pressure gradient ($\beta > 0$) these three distinct flow responses cease to exist and the low-speed streak structures present in the second and third regimes very rapidly disappear, as shown in the right-hand column of Fig. 2 for $\beta = 0.1$. The removal of streamwise-aligned streaks greatly reduces the radial flow into the far field in the (ζ, η) plane, corresponding to a reduction in the magnitude of the mass flux parameter A defined by (12), which we demonstrate must be such that $A = O(\zeta_0)$ for $\beta > 0$.

Far from the injection slot ($\hat{\zeta} \gg 1$) the flow remains unaffected by the ($\hat{\zeta} = O(1)$) injection-slot region, resulting in a two-dimensional solution of Falkner–Skan type. This solution has no cross flow at leading order ($O(\zeta_0)$) and can be continued from large $\hat{\zeta}$ towards $\hat{\zeta} = 0$ by parabolic marching of (15). For sufficiently favourable pressure gradients, $\beta_c(K) < \beta < 1$, this results in good agreement with the full numerical solution of (6) outside of a viscous-dominated layer that straddles the edge of the injection region. For weakly favourable pressure gradients $0 < \beta < \beta_c(K)$, we still find good agreement with the numerical solution, but this agreement fails dramatically near the centreline of the injection slot.

This study therefore highlights some fundamental qualitative differences associated with the presence of both short-spanwise scales and a favourable streamwise pressure gradient. For a strongly favourable pressure gradient, above the critical value $\beta_c(K) < \beta < 1$, any residual cross flow does not grow in the injection region and as the slot is widened, one simply recovers the classical Falkner–Skan solution local to the centreline. However, for $0 < \beta < \beta_c(K)$ any residual cross flow becomes increasingly important on approaching the centreline. Mathematically this behaviour arises through the appearance of a spatially unstable eigenmode as $\hat{\zeta} \to 0$. Crucially the eigenfunction of this 'unstable' mode has non-zero cross flow, and so it is only triggered by the higher-order corrections for large slot widths. A practical consequence of this behaviour is that the limit of wide injection slots in this 'micro-slot' formulation only recovers the Falkner–Skan solution for $\beta_c(K) < \beta < 1$. If $0 < \beta < \beta_c(K)$ an increasingly wide injection slot results in a cross-flow entrainment of fluid from outside the injection slot and its transport towards the centreline of the slot. For $0 < \beta < \beta_c(K)$ this cross flow leads to collisional behaviour along the centreline of the slot, which is in turn associated with a thin $\hat{\zeta} \ll 1$ eruption region as the slot widens ($\zeta_0 \gg 1$).

References

1. Kumar V, Alvi FS (2006) Use of high-speed microjets for active separation control in diffusers. AIAA J 44(2):273–281
2. van Dommelen LL, Yapalparvi R (2014) Laminar boundary-layer separation control by Görtler-scale blowing. Eur J Mech B 46:116
3. Catherall D, Stewartson K, Williams PG (1965) Viscous flow past a flat plate with uniform injection. Proc R Soc Lond A 284(1398):370396
4. Patankar SV, Spalding DB (1972) A calculation procedure for heat, mass and momentum transfer in three-dimensional parabolic flows. Int J Heat Mass Transf 15(10):1787–1806
5. Patankar S (1980) Numerical heat transfer and fluid flow. CRC Press, Boca Raton
6. Kemp NH (1951) The laminar three-dimensional boundary layer and a study of the flow past a side edge. M.Ae.S. thesis Cornell University
7. Goldstein ME, Sescu A, Duck PW, Choudhari M (2010) The long range persistence of wakes behind a row of roughness elements. J Fluid Mech 644:123–163
8. Goldstein ME, Sescu A, Duck PW, Choudhari M (2016) Nonlinear wakes behind a row of elongated roughness elements. J Fluid Mech 796:516–557
9. Ricco P, Dilib F (2010) The influence of wall suction and blowing on boundary-layer laminar streaks generated by free-stream vortical disturbances. Phys Fluids 22(4):044101

10. Hartree DR (1937) On an equation occurring in Falkner and Skan's approximate treatment of the equations of the boundary layer. Math Proc Cam Philos Soc 33:223–239
11. Kassoy DR (1970) On laminar boundary layer blowoff. SIAM J Appl Math 18(1):2940
12. Kassoy DR (1974) A resolution of the blow-off singularity for similarity flow on a plate. J Fluid Mech 62:145–161
13. Watson EJ (1966) The equation of similar profiles in boundary-layer theory with strong blowing. Proc R Soc Lond A 294(1437):208234
14. Hewitt RE, Duck PW, Williams A (2017) Injection into boundary layers: solutions beyond the classical form. J Fluid Mech 822:617–639
15. Dhanak MR, Duck PW (1997) The effects of freestream pressure gradient on a corner boundary layer. Proc R Soc Lond A 453:1793–1815
16. Pal A, Rubin SG (1971) Asymptotic features of viscous flow along a corner. Q Appl Math 29(1):91–108
17. Duck PW, Stow SR, Dhanak MR (2000) Boundary-layer flow along a ridge: alternatives to the Falkner–Skan solutions. Philos Trans R Soc Lond A 358(1777):3075–3090
18. Falkner VM, Skan SW (1930) Some approximate solutions of the boundary layer equations. Aero Res Council Lond Rep Mem, 1314
19. Hewitt RE, Duck PW (2014) Three-dimensional boundary layers with short spanwise scales. J Fluid Mech 756:452–469
20. Guennebaud G, Benoît J (2010) Eigen v3. http://eigen.tuxfamily.org
21. Kubota T, Fernandez FL (1968) Boundary-Layer flows with large injection and heat transfer. AIAA J 6(1):22–28